Effects of cellulose-lignin interaction on the evolution of biomass pyrolysis bio-oil heavy components

Yi Qiu, Dian Zhong, Kuo Zeng, Jun Li, Gilles Flamant, Ange Nzihou, Haiping Yang, Hanping Chen

Effects of cellulose-lignin interaction on the evolution of biomass pyrolysis bio-oil heavy components

Yi Qiu [a], Dian Zhong [b], Kuo Zeng [a,b,c,*], Jun Li [b], Gilles Flamant [d], Ange Nzihou [e], Haiping Yang [b], Hanping Chen [b]

[a] China-EU Institute for Clean and Renewable Energy, Huazhong University of Science and Technology, Wuhan 430074, PR China
[b] State Key Laboratory of Coal Combustion, Huazhong University of Science and Technology, 1037 Luoyu Road, Wuhan, Hubei 430074, PR China
[c] Shenzhen Huazhong University of Science and Technology Research Institute, Shenzhen 523000, PR China
[d] Processes, Materials and Solar Energy Laboratory, PROMES-CNRS, 7 rue du Four Solaire, 66120 Odeillo Font Romeu, France
[e] Université de Toulouse, Mines Albi, UMR CNRS 5302, Centre RAPSODEE, Campus Jarlard, F-81013 Albi cedex 09, France

A B S T R A C T

Cellulose, lignin and their mixture were pyrolyzed at 500–700 °C for 60 s and 90 s to investigate the influence of cellulose-lignin interaction on the evolution of biomass pyrolysis bio-oil heavy components with temperature and reaction time. Fourier transform-ion cyclotron resonance-mass spectrometry (FT-ICR-MS) and Fourier transform infrared spectroscopy (FT-IR) were used to characterize the composition and main functional groups of the heavy oil. Strong interaction among cellulose and lignin was revealed, which promoted the generation of lipids and unsaturated hydrocarbons while inhibiting the generation of the condensed aromatic hydrocarbons, phenolic species and sugars in the heavy components. With the use of van Krevelen diagrams, three reaction pathways are proposed to explain the evolution of heavy species under the influence of interaction, which is strongly affected by the removal of oxygen containing functional groups.

1. Introduction

Fast pyrolysis techniques have been widely used to transform lignocellulosic biomass into high value-added bio-oil, which can be further processed to produce electricity, heat, bio-fuels, carbon materials or chemicals [1–3]. However, the heavy components (with molecular weight > 200 Da) produced during the pyrolysis process remain the main issue to value-added bio-oil usage [4,5]. The high viscosity of bio-oil due to the existence of heavy components normally causes the contamination of the reactor and the deactivation of the catalyst [6]. Moreover, the oxygen abundant heavy components are highly reactive, non-volatile and easy to polymerize when heated, resulting in the thermal and chemical instability of bio-oil and the corrosion of equipment [7,8]. Therefore, to better utilize bio-oil in the future, it is of great significance to clarify the composition and formation mechanism of the heavy compounds.

Lignocellulosic biomass is usually regarded to be formed through cross-linking of three major components (cellulose, hemicellulose and lignin) that demonstrate different properties and behaviors during the pyrolysis process [3,9]. The influence of their interaction matters a lot during biomass pyrolysis [10–12]. Wu et al. reported that cellulose-lignin interaction enhanced the formation of low weight molecular products and proposed a possible interaction mechanism [11,13,14]. Hosoya et al. found that during co-pyrolysis, lignin inhibited the thermal polymerization of levoglucosan (mainly from cellulose) while cellulose enhanced the formation of some lignin-derived products (guaiacol, 4-methylguaiacol and 4-vinylguaiacol) [12]. They further proposed a possible interaction mechanism where the cellulose-derived volatiles act as H-donors and the lignin-derived volatiles act as H-acceptors [15]. These studies have presented valuable insights into the interaction mechanism of biomass three major components during pyrolysis, though it still remains a controversial topic [11]. In addition, most of the previous studies mainly focused on substances with small molecular weight using gas chromatography mass spectrometry (GC–MS), ultraviolet fluorescence (UV-F) spectroscopy, nuclear magnetic resonance (NMR) or gel permeation chromatography (GPC) [16–18], all of which are not adapted for effective analysis of the heavy components due to their high molecular weight and nonvolatility [19–21]. Therefore, more

* Corresponding author.
E-mail addresses: gilles.flamant@promes.cnrs.f (G. Flamant), ange.nzihou@mines-albi.fr (A. Nzihou), yhping2002@163.com (H. Yang), hp.chen@163.com (H. Chen).

Table 1
The proximate and ultimate analysis (dry basis, wt.%). V, FC and A represent volatile, fixed carbon and ash respectively.

	Proximate analysis			Ultimate analysis					LHV (MJ/kg)
	V	FC	A	C	H	N	S	O[a]	
Cellulose	95.5	4.5	0.0	42.7	6.2	0.03	0.05	51.0	15.47
Lignin	58.9	36.9	4.2	48.3	4.9	0.1	3.1	43.6	19.31

[a] Calculated by difference.

detailed chemical composition of the heavy components should be further identified.

The electrospray ionization Fourier transform ion cyclotron resonance mass (ESI FT-ICR-MS) spectrometry is known for its ultrahigh resolving power (>200,000) and wide detectable range (molecular weight of 200–1000 Da) [22–24]. Due to these advantages, the ion mass detected by the FT-ICR-MS can be used to calculate the accurate chemical formula of each heavy component [25,26]. With the use of FT-ICR-MS, Xiao et al. [27] explored the formation mechanism of the oxygenated polycyclic aromatic hydrocarbons during cellulose pyrolysis. Xiong et al. [20,21] revealed the significance of oxygen-containing functional groups during the formation of bio-oil heavy compounds. Li et al. [23] explored the evolution of nitrogen-containing species in the heavy components of algae pyrolysis bio-oil and found that N-containing components become more aromatic with rising temperature. These studies have successfully applied FT-ICR-MS into the investigation of bio-oil heavy components and proved its accuracy and effectivity. In our previous study [24], bio-oil heavy components from the pyrolysis of cellulose, hemicellulose and lignin were investigated using FT-ICR-MS and Kendrick mass defect (KMD) analysis. In terms of evolution pathways of bio-oil heavy compounds, obvious similarities between cellulose and hemicellulose, as well as large differences between holocellulose and lignin were revealed [24]. However, the interaction of cellulose and lignin in their pyrolysis heavy components has not been investigated yet.

In the present research, the physical mixture of cellulose and lignin was pyrolyzed at 500, 600 and 700 °C for 60 s and 90 s to investigate the effects of temperature and reaction stage on the co-pyrolysis heavy components. Meanwhile, cellulose and lignin were pyrolyzed independently to check the results without interaction. The comparison between co-pyrolysis results and independent pyrolysis results allowed deducing the effects of cellulose-lignin interaction. The van Krevelen diagram are used for data visualization, which sorts heavy components into different classes and makes it possible to investigate possible reaction pathways through linkages on the diagrams [28–30]. In addition to FT-ICR-MS analysis, FT-IR analysis was also used to reveal the changes of functional groups.

2. Materials and methods

2.1. Materials

The cellulose sample (CAS 9004-34-6) and alkali lignin (CAS 8068-05-1) were purchased from Sigma-Aldrich Pte. Ltd. (with purity ≥ 95%) and dried at 105 °C for 4 h before used. The cellulose and lignin samples were mixed with a mass ratio of 1:1 and milled using a planetary ball mill (PM 100, Germany) operating at a speed of 400 r/min for 15 min to form a physical mixture. In the following paragraphs, results derived from the pyrolysis of cellulose sample, lignin sample and cellulose-lignin mixture are labeled “C” “L” and “CL”, respectively. The proximate and ultimate analyses of the two basic components are shown in Table 1. The N and S contents of lignin are significantly higher than those of the cellulose, while its oxygen content is relatively lower. This

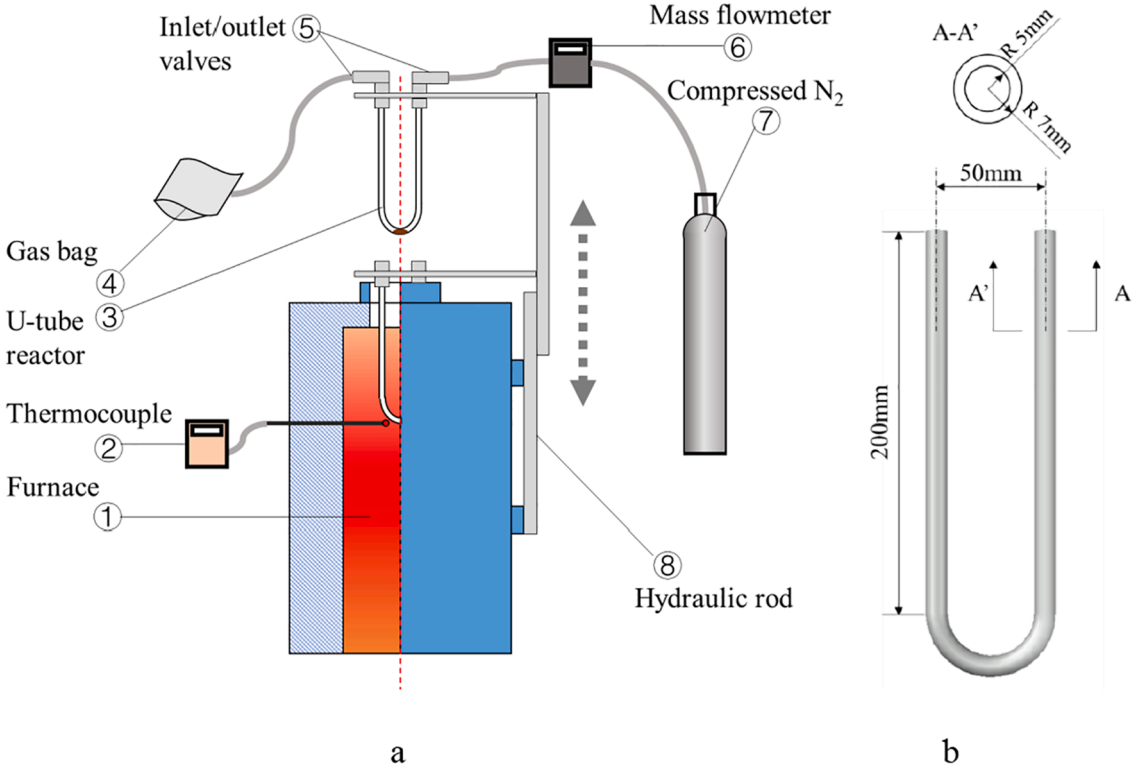

Fig. 1. The closed pyrolysis system (a) and the U-tube reactor (b).

Table 2
The rules applied for assignment of chemical formulas.

Items	Rules	Reference
C number	$^{12}C \leq 50$; $^{13}C \leq 2$	[38]
H number	$^{1}H \leq 100$; H/C ≤ 2.35	
O number	$^{16}O \leq 30$; O/C ≤ 2	
N number	$^{14}N \leq 5$;	
S number	$^{32}S \leq 2$; $^{35}S \leq 1$	
Relative error (ppm)	≤ 3 ppm	[20]
Absolute error	$\leq 10^{-3}$	[23]
DBE (Double Bond Equivalent)	Positive integer	[39]
Others	N-rules	[40]

difference has a great impact not only on the subsequent data processing but also on its pyrolysis behavior.

2.2. Experimental methods

The experiment was conducted in a closed reaction system shown in Fig. 1a. The system includes a vertical tube furnace (OTF-1200X-4-VTQ) and a quartz U-tube reactor. The specific size of the reactor is shown in Fig. 1b.

Before pyrolysis, 100 mg sample was loaded in the U-tube reactor, and then the system was flushed by N_2 (99.999%, 300 ml/min) for 3 min. The thermocouple was placed at a depth of 250 mm from the entrance of the furnace to measure the temperature of reaction zone. Once the target temperature was reached (500 °C, 600 °C, 700 °C), the gas inlet and outlet valves were closed immediately, and the reactor was quickly lowered down for pyrolysis. With small reactor size and sample amount, the heat transfer is considered very quick compared with reaction time. Hosoya and Jiang [31,32] found that the secondary reactions mainly take place after 60 s of pyrolysis for a small amount (100 mg) of cellulose and lignin, and that the pyrolysis is nearly completed after heating for 90 s or longer. Accordingly, the reaction time were set as 60 s and 90 s to represent the primary pyrolysis and secondary pyrolysis respectively. It should be noted that the threshold of reaction time is not absolute and may depend on different reactor configuration.

After pyrolysis for the setting time length (60 s, 90 s), the reactor was taken out immediately and cooled with compressed air for 2 min and subsequently immersed in ice-water mixture for 1 min. Then the valves were open again, allowing uncondensed gas to be wiped out by N_2 (99.999%, 300 ml/min) for 3 min. The gas was gathered by gas bag for further analysis. The liquid products condensed in the reactor was extracted with CH_3OH (LC/MS grade, purity $\geq$ 99.9%) to form a 10 ml solution. The dark-colored residue that cannot be dissolved as well as the solid product were together defined as char fraction in this paper.

2.3. Product analysis

2.3.1. Gas products

The gas products were qualitatively and quantitatively analyzed using a dual-channel micro-gas chromatography (Panna A91 GC) equipped with a thermal conductivity detector (TCD) and a hydrogen flame ionization detector (FID).

2.3.2. FT-ICR-MS analysis

FT-ICR-MS (Bruker, Solarix 7.0 T) was used to analyze the heavy compounds in bio-oil in negative mode using electrospray ionization (ESI) source, which has been reported effective for polar compounds (N, O, and S heteroatoms) in MS analysis [20,33]. Furthermore, the negative ion mode (ESI(-)) was chosen instead of the positive one (ESI(+)) because the bio-oil obtained from model compounds has little nitrogen and sulfur, which are preferred by ESI(+) [23]. The details of basic instrument setting have been mentioned in our previous study [23]. Before analysis, the bio-oil was diluted with CH_3OH (LC/MS grade) to 0.4 mg/ml for a better ionization and separation in the FT-ICR-MS [34–36], and the instrument was calibrated by NaCOOH (≥99.99%) solution [37]. Then the sample was infused into the MS at a rate of 120 μml/h. Each spectrum was gained after co-adding 128 scans to enhance the signal-to-noise ratio (S/N).

After acquisition, the mass spectra data were loaded into Bruker DataAnalysis 4.2 software for calibration. The full scan mass spectra were internally calibrated using a series of homologous compounds throughout the detected *m/z* range. Elemental formulas were assigned to the peaks inside the calibrated *m/z* range. The signals with a ratio of signal to noise (S/N) $\geq$ 3 were selected [21] for further assignment using MATLAB script with tolerances listed in Table 2 to filter the formulas [23]. Besides, the solvent used to dilute the oil sample was also analyzed, and the prominent signals in solvent mass spectrum were abandoned in the experiment results.

2.3.3. FT-IR analysis

Fourier transform infrared spectroscopy (FT-IR) technique is frequently used to identify the main functional groups present in bio-oil compounds [41,42]. In this study, a Fourier transform infrared spectroscopy (INVENIO-R, Bruker, Germany) was used to perform 32 scans

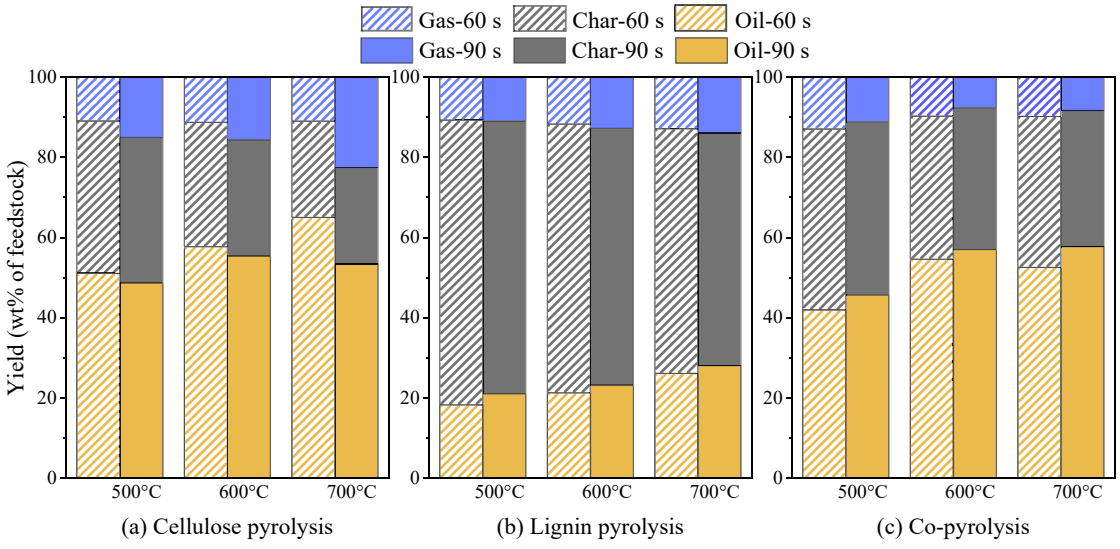

Fig. 2. Yields of bio-oil, char and gas from cellulose pyrolysis, lignin pyrolysis and co-pyrolysis (bio-oil yields are calculated by difference).

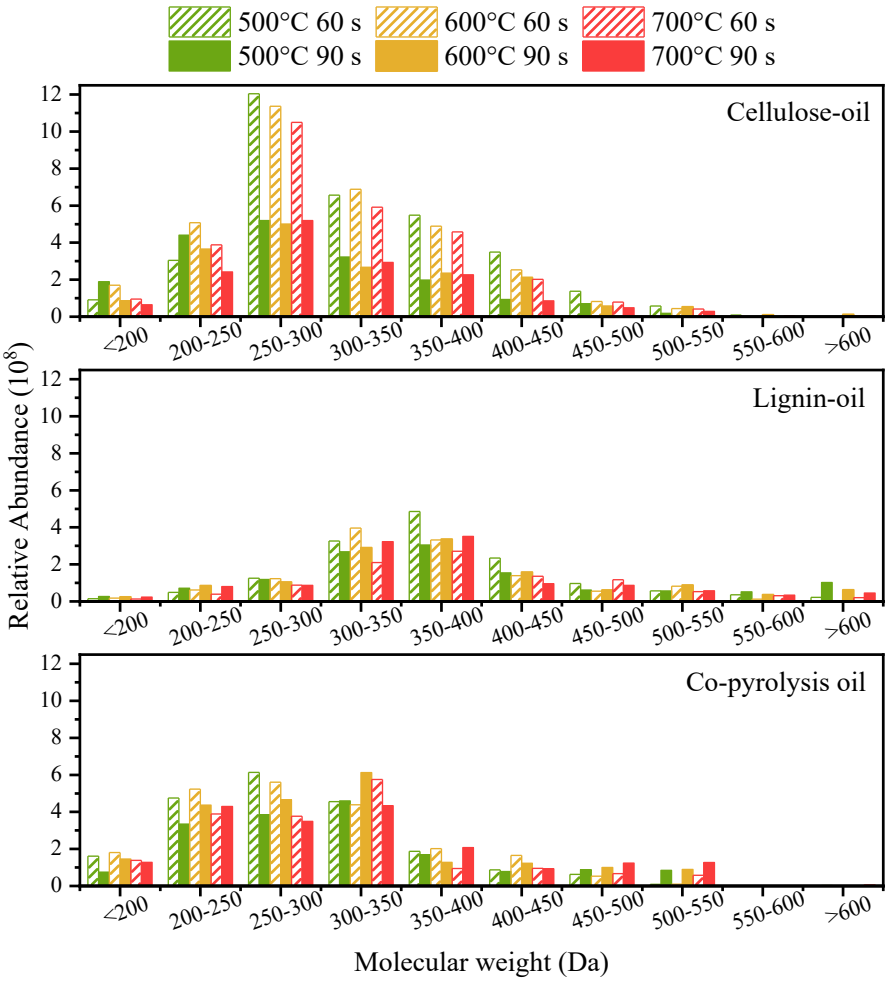

Fig. 3. Mass distributions of heavy components from the cellulose-oil, lignin-oil and co-pyrolysis oil.

with 4 cm^{-1} resolution between 400 cm^{-1} and 4000 cm^{-1} to determine the functional groups of the bio-oil samples.

3. Results and discussion

3.1. Final product distribution

In general, the co-pyrolysis results resemble the cellulose pyrolysis results rather than the average of cellulose and lignin pyrolysis (Fig. 2). Oil yields are lower than 25% in lignin pyrolysis for all groups, while they are between 40%~60% in both cellulose pyrolysis and co-pyrolysis. Lignin pyrolysis produces the highest char yields (64.8% on average), which are reduced sharply to 38.5% on average during co-pyrolysis, much closer to the cellulose pyrolysis results (30.4% on average). These indicate that interaction between cellulose and lignin actually promotes oil yields and inhibits char formation.

Rising temperature causes obvious increase in oil yields from cellulose pyrolysis and co-pyrolysis. Extending reaction time from 60 s to 90 s promotes oil-yields from lignin pyrolysis and co-pyrolysis while inhibiting those from cellulose pyrolysis. Secondary reaction was reported to reduce the oil yield of cellulose [43,44]. However, during co-pyrolysis, radicals from cellulose could enhance the secondary tar formation from lignin [45,46], leading to higher oil-yields in 90 s co-pyrolysis groups. Changes of gas and char yields are not further discussed.

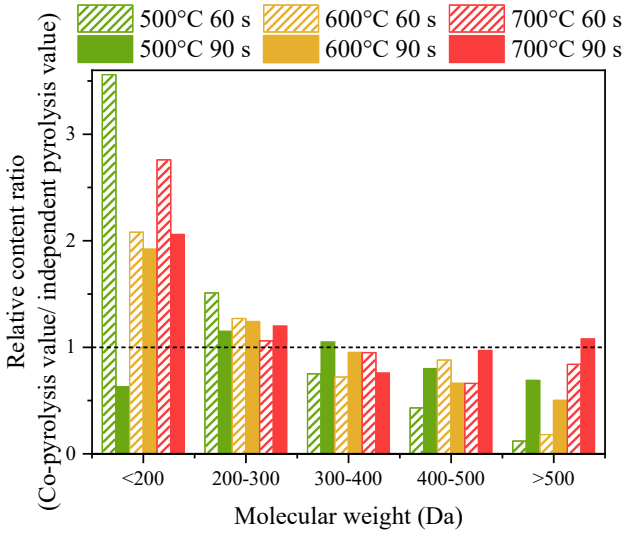

Fig. 4. Effects of cellulose-lignin interaction on mass distributions, marked by relative content ratio (co-pyrolysis value/ independent pyrolysis value).

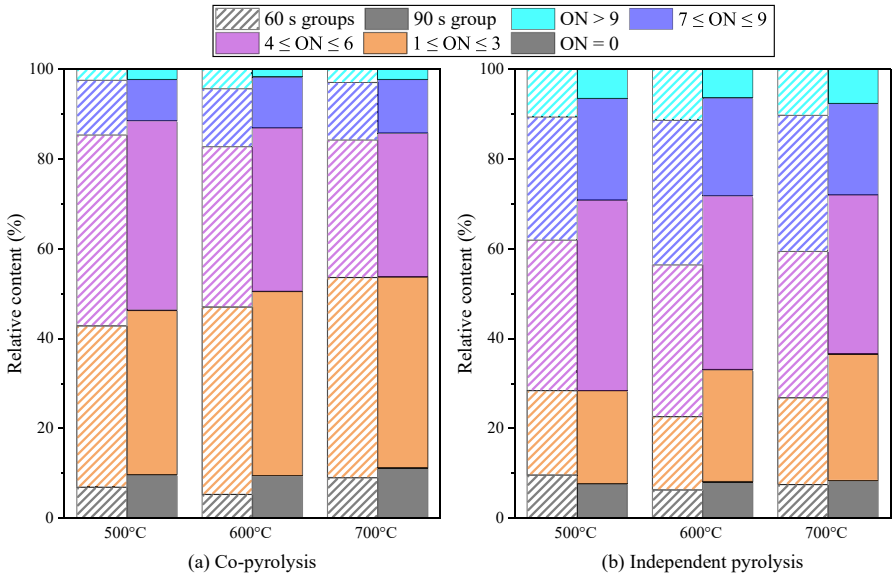

Fig. 5. Percentages of different O-containing species in heavy compounds in (a) co-pyrolysis oil and (b) independent pyrolysis results at 500, 600 and 700 °C for 60 s and 90 s.

3.2. Evolution of mass distribution and elementary composition

Quasi-normal distributions are observed in the mass distributions of both cellulose and lignin heavy components as shown in Fig. 3, with main molecular weights (MW) in the range of 250–300 Da and 300–400 Da, respectively. The heavy components from co-pyrolysis, however, distribute more evenly in the concentrating area of 200–350 Da. With the extension of reaction time to 90 s, the co-pyrolysis heavy

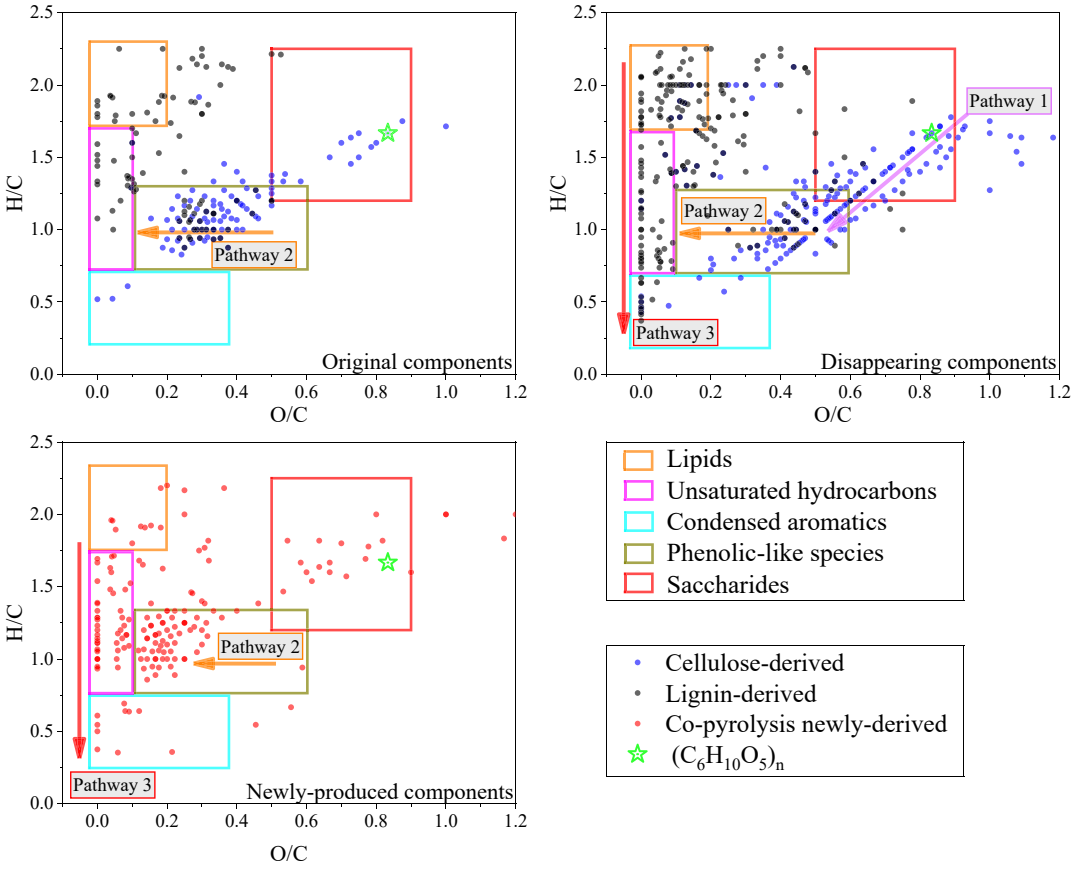

Fig. 6. Bio-oil heavy components of different origins in the van Krevelen diagrams, with original components and disappearing components sub-divided into cellulose-derived and lignin-derived components, respectively.

components with MW less than 300 Da reduced largely and more heavy components with MW of 450–550 Da were produced, which is attributed to the re-polymerization of the released volatiles in the secondary pyrolysis stage [21]. Besides, as temperature rises, the abundance in the larger MW range (especially in 500–550 Da) grows rapidly, indicating that higher temperature also has a promoting effect on the re-polymerization, as found in previous literature [47].

Fig. 4 further demonstrates the effects of cellulose-lignin interaction on mass distribution. Interaction promotes generation of substances with relative content ratios greater than one and vice versa. Components with molecular weight less than 300 Da are obviously promoted by interaction, although the effect is weakened with the extension of pyrolysis time. Lignin or lignin-derived products might promote cellulose cracking or the decomposition of low MW products from cellulose, including anhydrosugars and furans [11]. Noticeably, the generation of heavy components with molecular weight higher than 450 Da are largely inhibited by the interaction. Because heavy components in this range are mainly produced by the pyrolysis of lignin (Fig. 3), it can be speculated that the existence of cellulose is inhibiting the lignin components from forming larger molecules.

The formation of bio-oil heavy compounds is significantly affected by the evolution of oxygen-containing species [21]. To demonstrate their evolution trends, the oxygen contents of heavy components are calculated according to Eq. (1) [24].

$$C_{ON=x} = \frac{\sum I(O_x)}{\sum I} \tag{1}$$

where ON stands for the number of oxygen atoms contained in each molecule, $C_{ON=x}$ represents the relative content of the compounds with x oxygen atoms, I is the peak abundance of each molecular detected, and $I(O_x)$ is the peak abundance of molecular with x oxygen atoms. The comparison of oxygen contents between co-pyrolysis and independent pyrolysis results is presented in Fig. 5, and the original data used to calculate independent pyrolysis results can be found in Table S1.

For the general distribution of O-containing species, obvious differences are observed (Fig. 5) between co-pyrolysis results and independent pyrolysis results, concentrating in the oxygen number (ON) range of 1–6 and spreading in a much larger range of 1–9 ON, respectively. Co-pyrolysis obviously reduces the generation of substances with ON greater than 7, while promoting the generation of those with ON less than 3. Previous results indicate that the interaction among cellulose and lignin can significantly promote the deoxygenation reactions of heavy components. The removal of O-containing functional groups of lignin volatiles, such as carbonyl and carboxyl, are accelerated by vapor-solid interactions between cellulose and lignin [48]. Moreover, with the extension of reaction time, both co-pyrolysis and independent pyrolysis groups show a similar trend of deoxygenation, as substances with high oxygen content (ON $\geq$ 7) share an ever-smaller percentage and species with lower oxygen content (ON $\leq$ 3) increase. These trends are more obvious in the co-pyrolysis group, especially for species with no oxygen content, which increase drastically (at most by 79.2% at 600 °C) from 60 s to 90 s.

3.3. Evolution of different species in heavy components

The graphical plot of H/C ratio versus O/C ratio of each compound detected by FT-ICR-MS is illustrated in the van Krevelen diagram (Fig. S1). Different classes of species are located in their unique constant regions on the van Krevelen diagram. According to the methods introduced by previous studies [28–30], they can be generally classified as lipids ($0 \leq O/C \leq 0.2$, $1.7 \leq H/C \leq 2.25$), unsaturated hydrocarbons (UHs, $0 \leq O/C \leq 0.1$, $0.7 \leq H/C$ less than 1.7), condensed aromatic hydrocarbons (CAHs, $0 \leq O/C \leq 1.0$, $0.3 \leq H/C \leq 0.7$), phenolic-like species ($0 \leq O/C \leq 0.6$, $0.6 \leq H/C \leq 1.3$) and saccharides (sugars, $0.5 \leq O/C \leq 0.9$, $1.2 \leq H/C \leq 2.25$). Characterization of different kinds of milled wood lignin with MALDI–FT-ICR-MS by Evan et al. [29] has shown almost all of the detected components are bounded roughly by 0.2–0.5 for O/C and 0.8–1.3 for H/C on van Krevelen diagram, completely within the region of phenolic-like species. It should be noted that this can only be roughly seen as a starting region of lignin before pyrolysis because of the complexity of lignin raw materials. As for cellulose, $(C_6H_{10}O_6)_n$ is considered as a representative starting point (H/C = 1.667 and O/C = 0.833) before pyrolysis (Fig. 6), which is very close with the average result calculated based on ultimate analysis in Table 1 (H/C = 1.742 and O/C = 0.896). After pyrolysis, the heavy compounds from the cellulose-oil are mainly distributed in the regions of sugars and phenolic-like species, while those from the lignin-oil concentrate mainly in the regions of lipids, unsaturated hydrocarbons and phenolic-like species (Fig. S1). On the whole, the diagrams of co-pyrolysis oil resemble the superimpositions of the cellulose-oil and lignin-oil, with abundant distributions in all regions except condensed aromatics. To better illustrate the influence of cellulose-lignin interaction, the compounds repeatedly emerging in Fig. S1 are sorted out and classified into three categories (Fig. 6): original components (detected in both co-pyrolysis experiments and independent pyrolysis of cellulose or lignin), disappearing components (detected in the independent pyrolysis of cellulose or lignin but not in the co-pyrolysis experiments) and newly-produced components (detected only in the co-pyrolysis experiments).

Table 3
Average physiochemical characteristics of phenolic-like species with different origins. ON: oxygen number.

Origins	Amount	MW	O/C	H/C	ON
Original	102	268.176	0.321	1.134	4.549
Disappearing	126	327.388	0.400	1.108	6.349
Newly-produced	71	278.824	0.231	1.167	3.606

Phenolic-like species are dominant in original components and are mainly derived from cellulose (Fig. 6). Since cellulose itself does not contain aromatic structures, phenolic-like species can only be produced through the depolymerization of polysaccharide precursors [49]. This reaction pathway (pathway 1) starts right from the raw cellulose as represented by its chemical formula (Fig. 6) and crosses all the way through the saccharides' region and phenolic-like region with a slope of H/O = 2, which corresponds to the loss of water molecules [28]. This indicates that the saccharides species in cellulose have a strong tendency of transforming into phenolic-like species through dehydration. Moreover, pathway 1 is found only in the plot of disappearing components, from which it is speculated that this reaction pathway is accelerated by the cellulose-lignin interaction. The phenolic-like species are located in different regions in different diagrams (Fig. 6), which is caused by their different O/C ratio (Table 3). During co-pyrolysis, both original components and disappearing components can act as the precursors of newly-derived components. Under the influence of interaction, the phenolic-like species in newly-derived components lose on average about one oxygen atom from original components and three oxygen atoms from disappearing substances. This reaction pathway is marked as pathway 2 in Fig. 6, which is corresponding to the loss of –OH or –COOH. Intensive distribution is spotted in the lipids' region of disappearing components, all derived from lignin-oil. Very few points are spotted in the same region of newly-produced components, which indicates that lignin-derived lipids undergo excessive transformation during co-pyrolysis. It is speculated that the condensation reaction promoted by interaction causes the lipids to evolve along pathway 3 (Fig. 6) to form unsaturated hydrocarbons and even condensed aromatics.

Different species of heavy components from Fig. S1 are further compared in terms of their abundance (Fig. 7). In the 60 s groups, as temperature rises, the lipids' abundances in independent pyrolysis decrease while those in co-pyrolysis increase (Fig. 6). When reaction time extends to 90 s, more lipids are generated in both independent

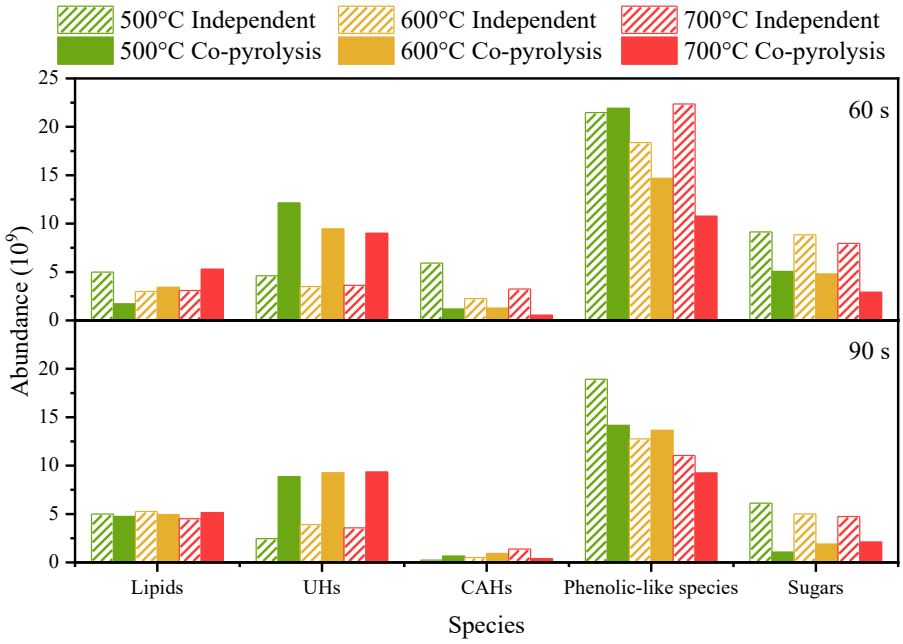

Fig. 7. Abundances of different species derived from independent pyrolysis and co-pyrolysis of different reaction time and temperature (UHs: unsaturated hydrocarbons; CAHs: condensed aromatic hydrocarbons).

Table 4
Summary of effects of interaction and longer reaction time on the abundance of different species in co-pyrolysis heavy components (+: promoted; ++: strongly promoted; -: inhibited; –: strongly inhibited).

Factors	Effects on different species				
	Lipids	UHs	CAHs	Phenolics	Sugars
Interaction	+	++	–	-	–
Longer reaction time	+	-	-	-	–

pyrolysis and co-pyrolysis. Lipids are mainly generated from the pyrolysis of lignin (Fig. 6), where the side chains are removed and recombined to form lipids and unsaturated hydrocarbons. The removal reactions on lignin side chains are likely to be completed with longer reaction time as the abundances of lipids become insensitive to both the changes of temperature and the co-pyrolysis with cellulose.

In all groups of temperature and reaction time (Fig. 7), the abundances of UHs in co-pyrolysis are more than twice of those in independent pyrolysis, indicating a significant promoting effect of interaction on UHs generation. Like lipids, UHs are also formed mainly through the side chains removal and recombination of lignin. The interaction with cellulose-derived small molecules (radicals) is likely to promote the removal of lignin side chains, thus producing more UHs, as was suggested by pathway 3 (Fig. 6). The CAHs produced in co-pyrolysis are much less than those produced in independent pyrolysis in terms of abundance, indicating strong interaction-inhibiting effects. During the co-pyrolysis, the generation of both UHs and CAHs is slightly inhibited when reaction time extends to 90 s. For phenolic-like species, extending reaction time results in obvious reduction of abundances in all temperature sets. Longer reaction time and higher temperature is likely to strengthen the evolution of components through pathway 2 (Fig. 6), which transforms phenolic-like species to UHs. This pathway is also promoted by higher temperature and cellulose-lignin interaction, as is suggested by the changes in abundances (Fig. 7). With the extension of time, less sugars are generated in both independent-pyrolysis oil and co-pyrolysis oil. Cellulose-lignin interaction significantly inhibited the generation of sugars, as the abundances of sugars are reduced largely during co-pyrolysis. These findings are in accordance with the pathway 1 in Fig. 6.

As a brief conclusion, effects of interaction and longer reaction time on the abundances of different species in co-pyrolysis heavy components are presented in Table 4. As can be spotted, interaction promotes the generation of lipids and unsaturated hydrocarbons, while inhibiting that of the condensed aromatic hydrocarbons, phenolic-like species and sugars. Longer reaction time also favors the generation of lipids while all other species are inhibited.

3.4. *Bulk physicochemical characteristics of the heavy components*

Table 6 shows the bulk physicochemical characteristics of bio-oil heavy components by calculating the average molecular weight (AMW), O/C ratio, H/C ratio and average double bond equivalent (ADBE) of co-pyrolysis heavy oil and independent pyrolysis value. The calculating methods have been previously reported [50]. Original data of individual pyrolysis can be found in Table S2.

The average molecular weight is in accordance with Fig. 3. It is worth noticing that the independent pyrolysis MW is higher than the co-pyrolysis MW in 60 s groups, while they show no big difference in 90 s groups, indicating that the decomposition promoting effects of interactions on heavy components mainly happen in the primary stage. The O/C of cellulose-oil is about two times as much as that of lignin, which is in accordance with the more abundant O-containing phenolic likes and sugars in cellulose-oil (Fig. S1). The co-pyrolysis O/C ratios are reduced largely compared with the O/C ratios of independent pyrolysis, which is more obvious in 90 s groups. Lignin-oil contains more UHs and lipids (Fig. S1), resulting in its higher H/C ratio. The co-pyrolysis H/C ratio (1.303 on average) is lower than the independent pyrolysis H/C ratio (1.362), indicating that the condensation polymerization of heavy components is promoted by the interaction.

Moreover, the condensed degree of the heavy components can be represented by the ADBE [51]. The co-pyrolysis ADBE (7.48 on average) is higher than the independent pyrolysis value (6.94 on average), which is mainly caused by more unsaturated hydrocarbons produced in the co-pyrolysis experiments (Fig. 7). As temperature rises, co-pyrolysis ADBE

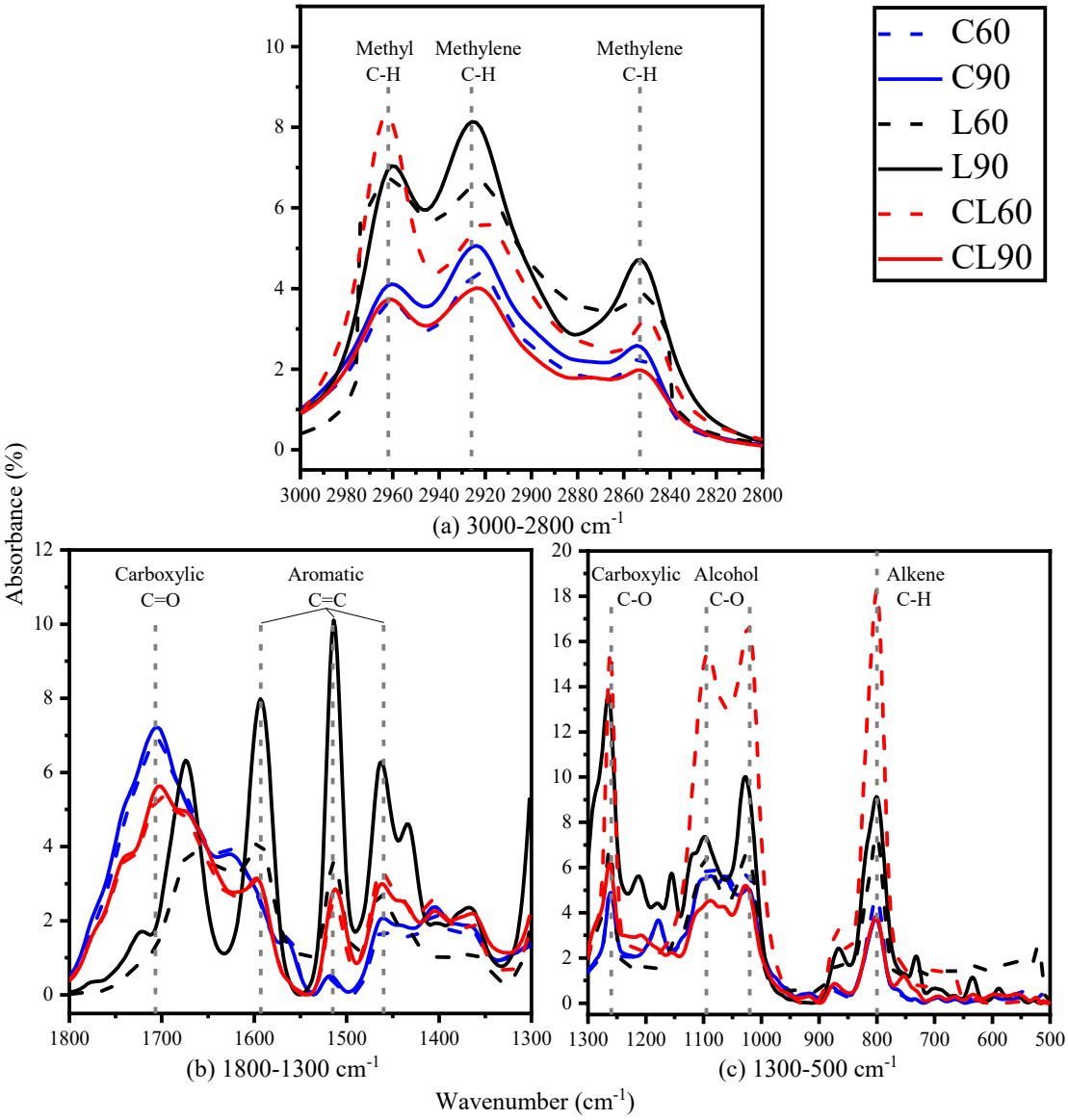

Fig. 8. FTIR absorbance spectra of bio-oil samples produced at 600 °C for 60 s and 90 s. Wavenumber scales: (a) 3000–2800 cm^{-1}, (b) 1800–1300 cm^{-1}, (c) 1300–500 cm^{-1}. C, L and CL represent cellulose-oil, lignin-oil and co-pyrolysis oil, respectively.

Table 5
Average physicochemical characteristics of heavy components in co-pyrolysis oil and independent pyrolysis results.

Sample	Time (s)	T (°C)	AMW	O/C	H/C	ADBE
Co-pyrolysis oil	60	500	315.72	0.274	1.278	7.88
		600	317.05	0.303	1.310	7.41
		700	313.29	0.265	1.271	7.00
	90	500	324.59	0.244	1.306	7.77
		600	316.45	0.257	1.288	7.75
		700	321.91	0.254	1.365	7.04
Independent pyrolysis results	60	500	352.77	0.306	1.332	7.88
		600	349.11	0.337	1.307	7.51
		700	345.12	0.331	1.308	7.73
	90	500	320.16	0.334	1.428	5.92
		600	316.75	0.313	1.403	5.90
		700	317.60	0.321	1.394	6.68

in both time sets drop down largely. This shows that high temperature generally promotes the decomposition of heavy components, causing the ADBE drop [21]. These results are also in good agreements with the previous finding that UHs and CAHs tend to be reduced at higher temperature.

Table 6
Types of vibrations and corresponding wavenumbers detected in FTIR spectroscopy process.

Wavenumbers (cm^{-1})	Types of vibrations	Functional groups	Ref.
2960	C–H (saturated) stretch	methyl	[52]
2930, 2850		methylene	[52]
1720–1703	C═O stretch	carboxylic acid	[54,55]
1593, 1515, 1460	C═C (aromatic)	aromatic	[54,56]
1260	C–O stretch	carboxylic acids	[55,57]
1095, 1020		alcohol	[55,57]
800	C–H (alkenes out-of-plane) bend	alkene	[55,58]

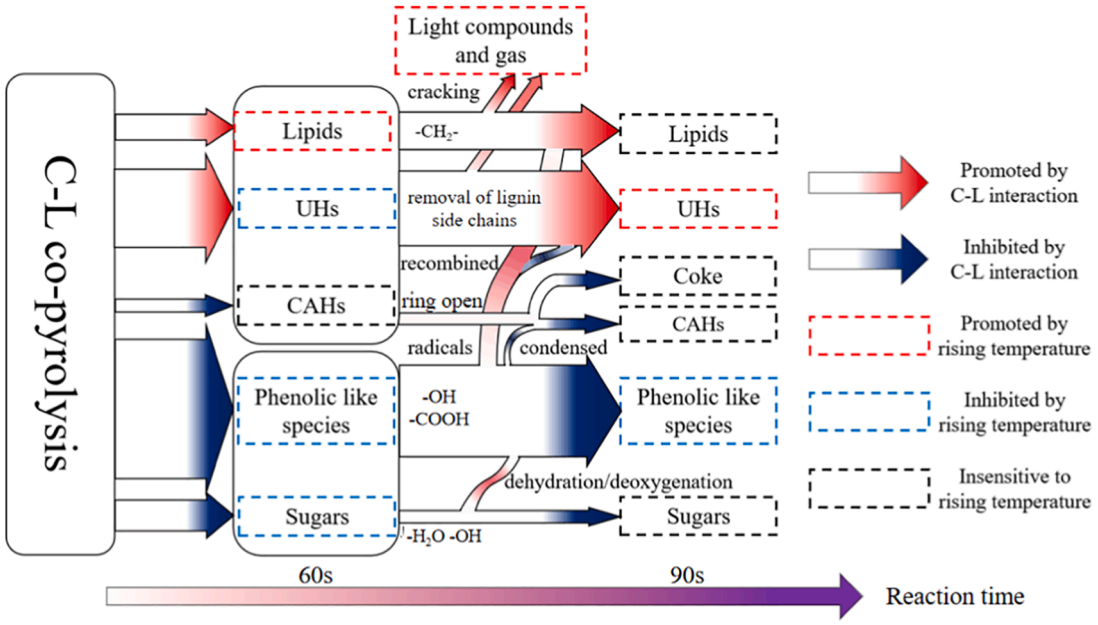

Fig. 9. The evolution of heavy compounds derived from co-pyrolysis of cellulose and lignin (UHs: unsaturated hydrocarbons; CAHs: condensed aromatic hydrocarbons).

3.5. FTIR analysis of bio-oils

The spectra are divided into eight groups of FTIR peaks indicating the main chemical functional groups of heavy oil identified during pyrolysis. The wavenumber ranges of these peaks and the corresponding types of vibrations are presented in Table 6 with their respective possible functional groups. The FTIR spectra is shown in Fig. 8. Wavenumber ranges of 4000–3000 cm^{-1} and 2800–1800 cm^{-1} are omitted because the peaks in these ranges are not significant or not discussed. The peaks at 2960, 2930 and 2850 cm^{-1} (Fig. 8a) are all linked to saturated C–H bond stretch [52]. They represent the existence of methyl (2960 cm^{-1}) and methylene (2930 and 2850 cm^{-1}) respectively. Lignin-oil has the highest peaks in accordance with its higher H/C ratio (Table 5). In the three curves of 90 s pyrolysis, the co-pyrolysis oil shows the lowest peak, which is also an obvious drop from the 60 s co-pyrolysis curve. This indicates that during the co-pyrolysis, methyl substituted groups of the heavy components could be demethylated [53] or the carbon chains have been broken down.

The C═O double bond stretching vibrations occur in the wavenumber range of 1900–1650 cm^{-1}, which are associated with aldehydes, acids, and esters groups [52]. In the present study, cellulose-oil shows the highest peaks at 1705 cm^{-1}, consistent with its highest oxygen content (Fig. 6). According to previous research [55], the C═O vibrations in the range of 1725–1700 cm^{-1} are caused by the C═O on the carboxylic acids in particular. The lignin-oil show less obvious peaks in this range, indicating low acids content in its heavy components, contrary to that of the cellulose-oil and co-pyrolysis oil. The vibration peaks of C═O double bond on esters are identified to be in the range of 1750–1735 cm^{-1} [59]. As the six curves all show no significant peak in this range, it can be thus speculated that the heavy components classified as lipids are mostly carboxylic acids instead of esters. The combination of peaks at 1593, 1515 and 1460 cm^{-1} (Fig. 8b) are due to aromatic C═C vibrations, representing the existence of aromatic rings [55,60]. Zheng et al. attributed the variation of peaks at 1463 cm^{-1} to the deformation in the benzene rings [56]. Abundant benzene ring structures are detected in lignin-oil, as it shows the highest peaks at 1593, 1515 and 1460 cm^{-1}, especially in 90 s groups. Much fewer benzene rings are detected in the cellulose-oil and co-pyrolysis oil than in the lignin oil (Fig. 8b). They tend to become more stable in the co-pyrolysis oil as the extension of time causes little change on the peaks. The benzene ring structures can be found in the CAHs and phenolic-like species in heavy oil and the abundance of both are reduced with the effects of interaction (Table 4).

According to previous literature [57], the C–O stretch in the wavenumber range of 1300–1000 cm^{-1} can be caused by alcohol, ethers, esters and carboxylic acids. Kotaiah et al. detected C–O peaks caused by carboxylic acids at 1220 cm^{-1} and C–O peaks caused by alcohols at 1100 cm^{-1} [55]. The strong peaks of co-pyrolysis oil at 1260 and 1095 cm^{-1} (Fig. 8c) can be thus classified as the carboxylic acids and alcohols, respectively. As reaction times extends, these two peaks are reduced significantly during co-pyrolysis, indicating the C–O breakages of carboxylic acids and alcohols among the ways of deoxygenation reactions. Intriguingly, the carboxylic C═O vibrations at 1725–1700 cm^{-1} show no big difference for different reaction time, indicating that the decarboxylation reactions are mainly through the removal of hydroxyl on carboxylic functional group. The vibrations in the range of 1000–650 cm^{-1} are attributed to C–H bending of double-bonded carbon atoms on alkenes [58]. Kotaiah et al. further confirmed that the peaks detected at 815 cm^{-1} are caused by alkenes [55]. In this study, peaks are detected at 800 cm^{-1} (Fig. 8c), which can also be attributed to the existence of unsaturated hydrocarbons. As the reaction time extends, a significant drop can be spotted in the co-pyrolysis oil at 800 cm^{-1}, indicating that the unsaturated hydrocarbons may experience hydrogenation during the secondary stage, causing the drop of ADBE (Table 5).

3.6. Cellulose-lignin interaction on the evolution of bio-oil heavy components.

The heavy components derived from the co-pyrolysis of cellulose and lignin at 500, 600 and 700 °C with different reaction times have been analyzed in the previous sections. Based on these results, the possible evolution routes of the heavy components are shown in Fig. 9. Most of the proposed evolution routes referring to the independent pyrolysis of cellulose and lignin have been reviewed in our previous study [24]. The effects of interaction revealed in this study are specially presented with different arrow colors. In addition, the width of arrows is proportional to the abundances of respective substances.

The UHs and phenolic like species are dominant in the primary stage.

The generation of UHs and lipids are mainly due to the side chains removal and recombination of lignin components, which are significantly promoted by the interaction with cellulose. During the secondary stage, sugars undergo dehydration and deoxygenation reaction. And phenolic-like species become the most active components and undergo cracking, condensation and homologous evolution. More lipids and unsaturated hydrocarbons (UHs) are produced by the recombination of radicals generated by the secondary reactions of phenolic-like species and sugars. More light compounds are produced, mainly due to the side chain cracking of lipids and UHs. These possible routes of evolution are significantly affected by reactant interaction and process temperature, which have also been demonstrated.

4. Conclusions

Cellulose-lignin interaction promotes biomass pyrolysis oil yields and changes the mass distributions of heavy components as the components generally become lighter during co-pyrolysis. With the help of van Krevelen diagrams, three reaction pathways are proposed to explain the evolution of heavy species under the influence of interaction. Interaction promotes the generation of lipids and unsaturated hydrocarbons, while inhibiting that of the condensed aromatic hydrocarbons, phenolic-like species and sugars. Longer reaction time favors the generation of lipids while all other species are inhibited. Both the interaction and the extension of reaction time promote the removal of O-containing functional group in heavy components, mainly through the decarboxyl and dehydroxyl reactions of phenolic species and sugars.

CRediT authorship contribution statement

Yi Qiu: Writing – original draft, Software, Visualization. **Dian Zhong:** Writing – review & editing, Methodology, Formal analysis. **Kuo Zeng:** Writing – review & editing, Methodology, Formal analysis. **Jun Li:** Investigation, Software. **Gilles Flamant:** Methodology, Formal analysis. **Ange Nzihou:** Investigation, Formal analysis, Visualization. **Haiping Yang:** Conceptualization, Resources, Validation. **Hanping Chen:** Validation.

Declaration of Competing Interest

The authors declare that they have no known competing financial interests or personal relationships that could have appeared to influence the work reported in this paper.

Acknowledgements

Authors acknowledge funding from the National Key R&D Program of China (2017YFE0124200), the National Natural Science Foundation of China (52076098), the International Cooperation Project of Shenzhen (GJHZ20190820102607238) and The Young Top-notch Talent Cultivation Program of Hubei Province. The FT-ICR-MS test was provided by Analytical & Testing Center of Huazhong University of Science & Technology. There are no conflicts to declare.

Appendix A. Supplementary data

Supplementary data to this article can be found online at https://doi.org/10.1016/j.fuel.2022.124413.

References

[1] Pires APP, Arauzo J, Fonts I, Domine ME, Arroyo AF, Garcia-Perez ME, et al. Challenges and Opportunities for Bio-oil Refining: A Review. Energy Fuels 2019;33(6):4683–720.
[2] Han Y, Gholizadeh M, Tran C-C, Kaliaguine S, Li C-Z, Olarte M, et al. Hydrotreatment of pyrolysis bio-oil: A review. Fuel Process Technol 2019;195:106140.
[3] Wang GY, Dai YJ, Yang HP, Xiong QG, Wang KG, Zhou JS, et al. A Review of Recent Advances in Biomass Pyrolysis. Energy Fuels 2020;34(12):15557–78.
[4] Gholizadeh M, Gunawan R, Hu X, Hasan MM, Kersten S, Westerhof R, et al. Different reaction behaviours of the light and heavy components of bio-oil during the hydrotreatment in a continuous pack-bed reactor. Fuel Process Technol 2016;146:76–84.
[5] Qin LY, Shao Y, Hou ZW, Jia YW, Jiang EC. Ultrasonic-Assisted Upgrading of the Heavy Bio-Oil Obtained from Pyrolysis of Pine Nut Shells with Methanol and Octanol Solvents. Energy Fuels 2019;33(9):8640–8.
[6] Nowakowska M, Herbinet O, Dufour A, Glaude PA. Detailed kinetic study of anisole pyrolysis and oxidation to understand tar formation during biomass combustion and gasification. Combust Flame 2014;161(6):1474–88.
[7] Chua YW, Yu Y, Wu HW. Thermal decomposition of pyrolytic lignin under inert conditions at low temperatures. Fuel 2017;200:70–5.
[8] Xiong Z, Syed-Hassan SSA, Hu X, Guo JH, Qiu JH, Zhao XY, et al. Pyrolysis of the aromatic-poor and aromatic-rich fractions of bio-oil: Characterization of coke structure and elucidation of coke formation mechanism. Appl Energy 2019;239:981–90.
[9] Yu HM, Zhang Z, Li ZS, Chen DZ. Characteristics of tar formation during cellulose, hemicellulose and lignin gasification. Fuel 2014;118:250–6.
[10] Collard FX, Blin J. A review on pyrolysis of biomass constituents: Mechanisms and composition of the products obtained from the conversion of cellulose, hemicelluloses and lignin. Renew Sustain Energy Rev 2014;38:594–608.
[11] Wu SL, Shen DK, Hu J, Zhang HY, Xiao R. Cellulose-lignin interactions during fast pyrolysis with different temperatures and mixing methods. Biomass Bioenergy 2016;90:209–17.
[12] Hosoya T, Kawamoto H, Saka S. Cellulose-hemicellulose and cellulose-lignin interactions in wood pyrolysis at gasification temperature. J Anal Appl Pyrol 2007;80(1):118–25.
[13] Wu SL, Shen DK, Hu J, Zhang HY, Xiao R. Intensive Interaction Region during Co-pyrolysis of Lignin and Cellulose: Experimental Observation and Kinetic Assessment. Bioresources 2014;9(2):2259–73.
[14] Wu SL, Shen DK, Hu J, Zhang HY, Xiao R. Cellulose-hemicellulose interactions during fast pyrolysis with different temperatures and mixing methods. Biomass Bioenergy 2016;95:55–63.
[15] Hosoya T, Kawamoto H, Saka S. Solid/liquid- and vapor-phase interactions between cellulose- and lignin-derived pyrolysis products. J Anal Appl Pyrol 2009;85(1–2):237–46.
[16] Bai XL, Kim KH, Brown RC, Dalluge E, Hutchinson C, Lee YJ, et al. Formation of phenolic oligomers during fast pyrolysis of lignin. Fuel 2014;128:170–9.
[17] Kadarwati S, Oudenhoven S, Schagen M, Hu X, Garcia-Perez M, Kersten S, et al. Polymerization and cracking during the hydrotreatment of bio-oil and heavy fractions obtained by fractional condensation using Ru/C and NiMo/Al2O3 catalyst. J Anal Appl Pyrol 2016;118:136–43.
[18] Xiong Z, Syed-Hassan SSA, Hu X, Guo JH, Chen YJ, Liu Q, et al. Effects of the component interaction on the formation of aromatic structures during the pyrolysis of bio-oil at various temperatures and heating rates. Fuel 2018;233:461–8.
[19] Hertzog J, Carre V, Jia LY, Mackay CL, Pinard L, Dufour A, et al. Catalytic Fast Pyrolysis of Biomass over Microporous and Hierarchical Zeolites: Characterization of Heavy Products. ACS Sustain Chem Eng 2018;6(4):4717–28.
[20] Xiong Z, Han HD, Azis MM, Hu X, Wang Y, Su S, et al. Formation of the heavy tar during bio-oil pyrolysis: A study based on Fourier transform ion cyclotron resonance mass spectrometry. Fuel 2019;239:108–16.
[21] Xiong Z, Guo J, Chaiwat W, Deng W, Hu X, Han H, et al. Assessing the chemical composition of heavy components in bio-oils from the pyrolysis of cellulose, hemicellulose and lignin at slow and fast heating rates. Fuel Process Technol 2020;199:106299.
[22] Terrell E, Garcia-Perez M. Novel Strategy To Analyze Fourier Transform Ion Cyclotron Resonance Mass Spectrometry Data of Biomass Pyrolysis Oil for Oligomeric Structure Assignment. Energy Fuels 2020;34(7):8466–81.
[23] Li J, Xiong Z, Zeng K, Zhong D, Zhang X, Chen W, Nzihou A, Flamant G, Yang HP, Chen HP. Characteristics and Evolution of Nitrogen in the Heavy Components of Algae Pyrolysis Bio-Oil (vol 55, pg 6373, 2021). Environ. Sci. Technol. 2021;55(16). 11465–11465.
[24] Zhong D, Zeng K, Li J, Qiu Y, Flamant G, Nzihou A, et al. Characteristics and evolution of heavy components in bio-oil from the pyrolysis of cellulose, hemicellulose and lignin. Renew Sustain Energy Rev 2022;157:111989.
[25] Tessarolo NS, Silva RVS, Vanini G, Casilli A, Ximenes VL, Mendes FL, et al. Characterization of thermal and catalytic pyrolysis bio-oils by high-resolution techniques: H-1 NMR, GC x GC-TOFMS and FT-ICR MS. J Anal Appl Pyrol 2016;117:257–67.
[26] Hertzog J, Mase C, Hubert-Roux M, Afonso C, Giusti P, Barrere-Mangote C. Characterization of Heavy Products from Lignocellulosic Biomass Pyrolysis by Chromatography and Fourier Transform Mass Spectrometry: A Review. Energy Fuels 2021;35(22):17979–8007.
[27] Xiao LF, Hu S, Song Y, Zhang LP, Han HD, Liu CY, et al. The formation mechanism for OPAHs during the cellulose thermal conversion in inert atmosphere at different temperatures based on ESI(-) FT-ICR MS measurement and density functional theory (DFT). Fuel 2019;239:320–9.
[28] Lozano DCP, Jones HE, Reina TR, Volpe R, Barrow MP. Unlocking the potential of biofuels via reaction pathways in van Krevelen diagrams. Green Chem 2021;23(22):8949–63.
[29] Terrell E, Carre V, Dufour A, Aubriet F, Le Brech Y, Garcia-Perez M. Contributions to Lignomics: Stochastic Generation of Oligomeric Lignin Structures for Interpretation of MALDI-FT-ICR-MS Results. ChemSusChem 2020;13(17):4428–45.

[30] Qi Y, Fu P, Li S, Ma C, Liu C, Volmer DA. Assessment of molecular diversity of lignin products by various ionization techniques and high-resolution mass spectrometry. Sci Total Environ 2020;713:136573.
[31] Hosoya T, Kawamoto H, Saka S. Pyrolysis gasification reactivities of primary tar and char fractions from cellulose and lignin as studied with a closed ampoule reactor. J Anal Appl Pyrol 2008;83(1):71–7.
[32] Jiang WK, Chu JY, Wu SB, Lucia LA. Modeling pyrolytic behavior of pre-oxidized lignin using four representative beta-ether-type lignin-like model polymers. Fuel Process Technol 2018;176:221–9.
[33] Hu S, Han HD, Syed-Hassan SSA, Zhang YN, Wang Y, Zhang LP, et al. Evolution of heavy components during sewage sludge pyrolysis: A study using an electrospray ionization Fourier transform ion cyclotron resonance mass spectrometry. Fuel Process Technol 2018;175:97–103.
[34] Cole DP, Smith EA, Dalluge D, Wilson DM, Heaton EA, Brown RC, et al. Molecular characterization of nitrogen-containing species in switchgrass bio-oils at various harvest times. Fuel 2013;111:718–26.
[35] Miettinen I, Makinen M, Vilppo T, Janis J. Compositional Characterization of Phase-Separated Pine Wood Slow Pyrolysis Oil by Negative-Ion Electrospray Ionization Fourier Transform Ion Cyclotron Resonance Mass Spectrometry. Energy Fuels 2015;29(3):1758–65.
[36] Stas M, Chudoba J, Auersvald M, Kubicka D, Conrad S, Schulzke T, et al. Application of orbitrap mass spectrometry for analysis of model bio-oil compounds and fast pyrolysis bio-oils from different biomass sources. J Anal Appl Pyrol 2017;124:230–8.
[37] Wang J, Hao ZN, Shi FQ, Yin YG, Cao D, Yao ZW, et al. Characterization of Brominated Disinfection Byproducts Formed During the Chlorination of Aquaculture Seawater. Environ Sci Technol 2018;52(10):5662–70.
[38] Ohno T, Ohno PE. Influence of heteroatom pre-selection on the molecular formula assignment of soil organic matter components determined by ultrahigh resolution mass spectrometry. Anal Bioanal Chem 2013;405(10):3299–306.
[39] Koch BP, Witt MR, Engbrodt R, Dittmar T, Kattner G. Molecular formulae of marine and terrigenous dissolved organic matter detected by electrospray ionization Fourier transform ion cyclotron resonance mass spectrometry. Geochim Cosmochim Acta 2005;69(13):3299–308.
[40] Koch BP, Dittmar T, Witt M, Kattner G. Fundamentals of molecular formula assignment to ultrahigh resolution mass data of natural organic matter. Anal Chem 2007;79(4):1758–63.
[41] Zhou J, Xiong Y, Gong YZ, Liu X. Analysis of the oxidative degradation of biodiesel blends using FTIR, UV-Vis, TGA and TD-DES methods. Fuel 2017;202:23–8.
[42] Aboulkas A, Hammani H, El Achaby M, Bilal E, Barakat A, El Harfi K. Valorization of algal waste via pyrolysis in a fixed-bed reactor: Production and characterization of bio-oil and bio-char. Bioresour Technol 2017;243:400–8.
[43] Shen DK, Gu S. The mechanism for thermal decomposition of cellulose and its main products. Bioresour Technol 2009;100(24):6496–504.
[44] Lanza R, Nogare DD, Canu P. Gas Phase Chemistry in Cellulose Fast Pyrolysis. Ind Eng Chem Res 2009;48(3):1391–9.
[45] Fushimi C, Katayama S, Tsutsumi A. Elucidation of interaction among cellulose, lignin and xylan during tar and gas evolution in steam gasification. J Anal Appl Pyrol 2009;86(1):82–9.
[46] Fushimi C, Katayama S, Tasaka K, Suzuki M, Tsutsumi A. Elucidation of the Interaction Among Cellulose, Xylan, and Lignin in Steam Gasification of Woody Biomass. AICHE J. 2009;55(2):529–37.
[47] Xiong Z, Wang Y, Syed-Hassan SSA, Hu X, Han HD, Su S, et al. Effects of heating rate on the evolution of bio-oil during its pyrolysis. Energy Convers Manage 2018;163:420–7.
[48] Yang H, Liu M, Chen Y, Xin S, Zhang X, Wang X, et al. Vapor-solid interaction among cellulose, hemicellulose and lignin. Fuel 2020;263:116681.
[49] Wang Q, Song H, Pan S, Dong NH, Wang XM, Sun SP. Initial pyrolysis mechanism and product formation of cellulose: An Experimental and Density functional theory (DFT) study. Sci Rep 2020;10(1).
[50] Zhang LP, Hu S, Chen QD, Han HD, Xiao LF, Xu J, et al. Identification of the structural characteristics of the asphaltenes in the tetrahydrofuran-microwave-extracted portions from two Chinese coals. Fuel Process Technol 2017;160:86–92.
[51] Stankovikj F, McDonald AG, Helms GL, Olarte MV, Garcia-Perez M. Characterization of the Water-Soluble Fraction of Woody Biomass Pyrolysis Oils. Energy Fuels 2017;31(2):1650–64.
[52] Barbosa JM, Andrade LA, Vieira LGM, Barrozo MAS. Multi-response optimization of bio-oil production from catalytic solar pyrolysis of Spirulina platensis. J Energy Inst 2020;93(4):1313–23.
[53] Zhang ZF, Huang K, Ye YJ, Shi JY, Zhang X. Pyrolysis Characteristics and Kinetics Analysis of Moso Bamboo. Materiale Plastice 2015;52(1):122–4.
[54] Liu J, Li RJ, Guo MY, Tao HR, Sun DL, Zong CX, et al. Study of the thermal degradation of benzene-containing glycerol carbonate derivatives by a combined TG-FTIR and theoretical calculation. Thermochim Acta 2017;654:179–85.
[55] Naik DK, Monika K, Prabhakar S, Parthasarathy R, Satyavathi B. Pyrolysis of sorghum bagasse biomass into bio-char and bio-oil products. J Therm Anal Calorim 2017;127(2):1277–89.
[56] Zheng YW, Tao L, Yang XQ, Huang YB, Liu C, Zheng ZF. Comparative study on pyrolysis and catalytic pyrolysis upgrading of biomass model compounds: Thermochemical behaviors, kinetics, and aromatic hydrocarbon formation. J Energy Inst 2019;92(5):1348–63.
[57] Peng XW, Ma XQ, Lin YS, Guo ZG, Hu SC, Ning XX, et al. Co-pyrolysis between microalgae and textile dyeing sludge by TG-FTIR: Kinetics and products. Energy Convers Manage 2015;100:391–402.
[58] Niu SL, Zhou Y, Yu HW, Lu CM, Han KH. Investigation on thermal degradation properties of oleic acid and its methyl and ethyl esters through TG-FTIR. Energy Convers Manage 2017;149:495–504.
[59] Marcilla A, Gomez-Siurana A, Gomis C, Chapuli E, Catala MC, Valdes FJ. Characterization of microalgal species through TGA/FTIR analysis: Application to nannochloropsis sp. Thermochim Acta 2009;484(1–2):41–7.
[60] Ogunkanmi JO, Kulla DM, Omisanya NO, Sumaila M, Obada DO, Dodoo-Arhin D. Extraction of bio-oil during pyrolysis of locally sourced palm kernel shells: Effect of process parameters, Case Studies in Thermal. Engineering 2018;12:711–6.